This article was downloaded by: [Renmin University of China]
On: 13 October 2013, At: 10:42
Publisher: Taylor & Francis
Informa Ltd Registered in England and Wales Registered Number: 1072954 Registered office: Mortimer House, 37-41 Mortimer Street, London W1T 3JH, UK

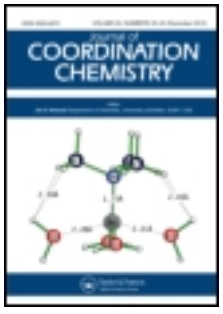

Journal of Coordination Chemistry
Publication details, including instructions for authors and subscription information:
http://www.tandfonline.com/loi/gcoo20

Synthesis, characterization, and solid state electrical conductivity of coordination polymers with copper and zinc

R.L. Prasad [a] & Anita Kushwaha [a]

[a] Department of Chemistry, Faculty of Science , Banaras Hindu University , Varanasi-221005 , India

Accepted author version posted online: 28 Sep 2012.Published online: 25 Oct 2012.

To cite this article: R.L. Prasad & Anita Kushwaha (2012) Synthesis, characterization, and solid state electrical conductivity of coordination polymers with copper and zinc, Journal of Coordination Chemistry, 65:23, 4230-4244, DOI: 10.1080/00958972.2012.733817

To link to this article: http://dx.doi.org/10.1080/00958972.2012.733817

PLEASE SCROLL DOWN FOR ARTICLE

Taylor & Francis makes every effort to ensure the accuracy of all the information (the "Content") contained in the publications on our platform. However, Taylor & Francis, our agents, and our licensors make no representations or warranties whatsoever as to the accuracy, completeness, or suitability for any purpose of the Content. Any opinions and views expressed in this publication are the opinions and views of the authors, and are not the views of or endorsed by Taylor & Francis. The accuracy of the Content should not be relied upon and should be independently verified with primary sources of information. Taylor and Francis shall not be liable for any losses, actions, claims, proceedings, demands, costs, expenses, damages, and other liabilities whatsoever or howsoever caused arising directly or indirectly in connection with, in relation to or arising out of the use of the Content.

This article may be used for research, teaching, and private study purposes. Any substantial or systematic reproduction, redistribution, reselling, loan, sub-licensing, systematic supply, or distribution in any form to anyone is expressly forbidden. Terms & Conditions of access and use can be found at http://www.tandfonline.com/page/terms-and-conditions

Journal of Coordination Chemistry
Vol. 65, No. 23, 10 December 2012, 4230–4244

Taylor & Francis
Taylor & Francis Group

Synthesis, characterization, and solid state electrical conductivity of coordination polymers with copper and zinc

R.L. PRASAD* and ANITA KUSHWAHA

Department of Chemistry, Faculty of Science, Banaras Hindu University, Varanasi-221005, India

(*Received 24 January 2012; in final form 13 August 2012*)

Heterobimetallic complexes $[Cu_xZn_{1-x}(dadb)\cdot yH_2O]_n$ {where dadb = 2,5-diamino-3,6-dichloro-1,4-benzoquinone (**1**); $x = 1$ (**2**), 0.5 (**4**), 0.25 (**5**), 0.125 (**6**), 0.0625 (**7**), and 0 (**3**); $y = 2$; n = degree of polymerization} were synthesized and characterized. All metal complexes are stable at room temperature but weakly absorb moisture on exposure to air. Monometallic **2** exhibits subnormal magnetic moment whereas **3** exhibits diamagnetism. Heterobimetallic complexes exhibit normal magnetic moments. Heterobimetallic complexes are characterized from powder X-ray diffraction, thermal analysis, and electron spin resonance (ESR) spectral studies. Delocalization of unpaired electron from metal to ligand has been inferred from ESR and natural bond orbital (NBO) analysis. Greater delocalization of unpaired electron of Cu(II) on ligand of **4** as compared to that of **2** is reflected from NBO analysis. Heterobimetallic complexes show higher conductivity than monometallic complexes; all the complexes exhibit semiconductor behavior.

Keywords: 1-D coordination polymer; Semiconductor; NBO charges; Metal complexes of 2,5-diamino-3,6-dichloro-1,4-benzoquinone; Heterobimetallic complexes; ESR spectra

Downloaded by [Renmin University of China] at 10:42 13 October 2013

1. Introduction

π-Conjugated polymers [1] as well as 1-D stacks of coordination polymers (KCP) [2, 3] are made highly conducting upon partial oxidation. In an idealized situation, a uniform chain of conjugated polymer possesses filled valence and empty conduction bands. On partial oxidation of the conjugated polymer the electron is removed from completely filled valence band giving a partially filled conduction band responsible for increase in conductivity. If the redox reagents are inhomogeneously distributed through the polymer chain side reactions occur on the polymeric backbone and yield saturated sites along the chain direction [4]. Side reactions on the polymer backbone inhibit the polymer's ability to achieve higher conductivity. Chemical treatment also adds impurities to the system, thereby reproducibility becomes difficult. Therefore, synthesis of good organometallic conductors by avoiding drawbacks of redox treatment is desirable and is a challenging task in materials chemistry.

*Corresponding author. Email: rlpjc@yahoo.co.in; rlp@bhu.ac.in

ISSN 0095-8972 print/ISSN 1029-0389 online © 2012 Taylor & Francis
http://dx.doi.org/10.1080/00958972.2012.733817

Zhu and Swager [5] reported that anchoring copper(II) along the conjugated polymeric chain increases the electrical conductivity of the conjugated polymers. Delocalization of unpaired electron from copper(II) onto the conjugated chain of ligands by forming metal-to-ligand π-back bonds is responsible for creation of partially filled bands increasing conductivity. This is supported by reports of electronic communication between two metal ions bridged by conjugated ligands [6–8]. Thus, a hybrid design incorporating conjugated polymer and metal ion having unpaired electron capable of forming metal-to-ligand back bonds may produce electrical conductance. Thus, metal ions having unpaired electrons are planned to be introduced into 1-D conjugated coordination polymeric chains to create a partially filled band in this work. Limitations arising from redox treatment have been carefully planned to create partially filled bands.

1-D coordination polymer $\{[Cu(CA)(H_2O)](H_2O)\}_n$ (CA = chloranilic acid) exhibits antiferromagnetic interactions [9, 10]. Antiferromagnetic interaction localizes the unpaired electrons and may hinder availability of unpaired electrons to form a conduction band along the conjugated chain direction. To avoid antiferromagnetic interaction between adjacent metal ions, the synthesis of 1-D coordination polymers bridged by conjugated ligand by diluting the magnetic nucleus (Cu(II)) by non-magnetic metal ions (Zn(II)) was undertaken. Results of this study give insights to design materials with electrical properties. Reports on metal complexes of dadb are lacking except a few by thermal study [11, 12]. In this communication, we report the solid state electrical conductivity of 1-D coordination polymers Cu_xZn_{1-x}(dadb) (where $x = 1.0$, 0.5, 0.25, 0.125, 0.0625, and 0).

Downloaded by [Renmin University of China] at 10:42 13 October 2013

2. Experimental

2.1. *Materials and methods*

All chemicals were of analytical reagent grade. Solvents were purified and dried prior to use by standard methods [13]. The 2,5-diamino-3,6-dichloro-1,4-benzoquinone (**1**) was prepared as described earlier [12, 14, 15].

2.2. *Syntheses of metal complexes*

2.2.1. Syntheses of complexes 2, 3, 4, and 7. Complexes **2**, **3**, **4**, and **7** were prepared as described earlier [11].

(a) $Cu(dadb) \cdot 2H_2O$ (**2**): Blackish green solid. Yield: 65%; m.p.: >280°C. Anal. Calcd for $Cu(C_6H_2O_2N_2Cl_2) \cdot 2H_2O$ (%): C, 23.65; H, 1.97; N, 9.19. Found (%): C, 24.24; H, 1.97; N, 8.63.

(b) $Zn(dadb) \cdot H_2O$ (**3**): Dark pink solid. Yield: 72%; m.p.: >300°C. Anal. Calcd for $Zn(C_6H_2O_2N_2Cl_2) \cdot H_2O$ (%): C, 24.97; H, 1.38; N, 9.71. Found (%): C, 25.54; H, 1.78; N, 9.24.

(c) $Cu_{0.5}Zn_{0.5}(dadb) \cdot 2H_2O$ (**4**): Gray solid. Yield: 84%; m.p.: 275–278°C dec. Anal. Calcd for $Cu_{0.5}Zn_{0.5}(C_6H_2O_2N_2Cl_2) \cdot 2H_2O$ (%): C, 23.57; H, 1.96; N, 9.17. Found (%): C, 22.95; H, 1.56; N, 8.74.

(d) $Cu_{0.0625}Zn_{0.9375}(dadb)\cdot 2H_2O$ (**7**): Gray solid. Yield: 66%; m.p.: 277–280°C dec. Anal. Calcd for $Cu_{0.0625}Zn_{0.9375}(C_6H_2O_2N_2Cl_2)\cdot 2H_2O$ (%): C, 23.51; H, 1.96; N, 9.14. Found (%): C, 23.93; H, 1.73; N, 8.70.

2.2.2. Synthesis of $Cu_{0.25}Zn_{0.75}(dadb)\cdot 2H_2O$ (5). Heterobimetallic **5** was synthesized by adding an aqueous solution of $ZnSO_4\cdot 7H_2O$ (0.431 g, 1.5 mmol) + $CuSO_4\cdot 5H_2O$ (0.125 g, 0.5 mmol) into a pink 50% ethanolic solution (40 mL) of dadb (0.414 g, 2 mmol) and KOH (0.224 g, 4 mmol) dropwise with constant stirring over a period of ½ h. The reaction mixture turned to an intense dark solution. The reaction mixture was further stirred for 5 h followed by digestion over a water bath for 30 min and cooled to room temperature. Resulting precipitate was filtered using suction and washed with distilled water. Precipitate was purified by stirring for 1 h in a solvent mixture of 25% ethanol, 25% acetone, 5% DMF, and 45% distilled water, filtered, washed with distilled water thrice followed by ethanol, and dried under vacuum over anhydrous $CaCl_2$. Light brown solid. Yield: 88%; m.p.: 282–285°C dec. Anal. Calcd for $Cu_{0.25}Zn_{0.75}C_6H_2O_2N_2Cl_2\cdot 2H_2O$ (FW 305.91) (%): Cu, 5.19; Zn, 16.02; C, 23.54; H, 1.96; N, 9.15. Found (%): Cu, 5.36; Zn, 16.8; C, 22.89; H, 1.42; N, 8.79.

2.2.3. $Cu_{0.125}Zn_{0.875}(dadb)\cdot 2H_2O$ (6). Heterobimetallic **6** was synthesized by adding an aqueous solution of $ZnSO_4\cdot 7H_2O$ (0.503 g, 1.75 mmol) and $CuSO_4\cdot 5H_2O$ (0.062 g, 0.25 mmol) into a pink 50% ethanolic solution (40 mL) of dadb (0.414 g, 2 mmol) and KOH (0.224 g, 4 mmol) dropwise with constant stirring over a period of ½ h. The procedure was the same as described for synthesis of **5**. Light gray solid. Yield: 83%; m.p.: 275–279°C dec. Anal. Calcd for $Cu_{0.125}Zn_{0.875}C_6H_2O_2N_2Cl_2\cdot 2H_2O$ (FW 306.14) (%): Cu, 2.59; Zn, 18.68; C, 23.51; H, 1.96, N, 9.15. Found (%): Cu, 1.76; Zn, 19.19; C, 23.01; H, 1.85; N, 9.0.

2.3. *Analyses and measurements*

Elemental analyses (carbon, hydrogen, and nitrogen) were performed on an Elemental Analyzer model Carlo Erba 1108. Copper and zinc analyses were performed by atomic absorption spectrophotometry using a Perkin Elmer AAnalyst-300 Spectrometer. Magnetic susceptibility of the powdered samples was measured at room temperature on a Cahn Faraday electro balance using $[Co(NCS)_4Hg]$ as calibrant. Melting points of the complexes were determined in open capillaries using a Gallenkamp apparatus and are uncorrected. Powder X-ray diffraction (PXRD) patterns were recorded at room temperature on a Rigaku miniflex II Desktop X-ray diffractometer with Cu-Kα radiation ($\lambda = 1.541836$ Å). Thermogravimetric analyses (TGA) were recorded on a Perkin Elmer thermal analyzer model Diamond TG/DTA and NETZSCH STA 409 C/CD. Electronic absorption spectra were recorded on a UV-1700 PHARMA SPEC UV-Visible spectrophotometer as Nujol mulls. IR spectra as KBR discs were recorded on a VARIAN 3100 FT-IR spectrophotometer from 4000 to 400 cm^{-1}. Room temperature electron spin resonance (ESR) spectra of powdered samples were recorded on a Varian, USA model E-112 ESR spectrometer. The microwave frequency was calibrated using tetracyanoethylene (TCNE), $g = 2.00277$. Variable temperature electrical conductivities of the complexes were measured using conventional two-probe

Downloaded by [Renmin University of China] at 10:42 13 October 2013

technique on a Keithley 236 source measure unit. Spherical pellets were prepared by putting the samples in a circular die with 13 mm diameter and applying a pressure of 6 ton. These pellets were cured at 110°C for 2 h in the laboratory oven and slowly cooled to 60°C in 1 h and finally cooled to room temperature in desiccators. Top and bottom surfaces of the cured pellets were coated with conductive silver paint purchased from Eltecks Corporation, Bangalore, to make electrical contacts. Variable temperature conductivity measurements were made by using indigenously made furnace by applying controlled current through a variac. Temperature of the sample was measured by a laboratory thermometer in its vicinity. Sequentially constant increasing voltage (in the range +10 to −10 V with an increase of 5 V in each step) was applied through the leads and the current across the leads was measured. Resistance was calculated from the slope of I/V curves. Specific resistance was calculated from resistance data using the known dimension of the pellets and converted into the specific conductance.

Downloaded by [Renmin University of China] at 10:42 13 October 2013

2.4. *Computational details*

Calculations of structural parameters and natural bond orbital (NBO) charges were carried out on a Pentium IV PC using windows version of Gaussian'03 suite of *ab initio* quantum chemical program [16]. Geometry of $Cu_2(\mu\text{-dadb})(dadbH)_2 \cdot 4H_2O$ and $Cu_2(\mu\text{-dadb})(dadbH)_2$ were optimized on b3lyp/cep-31 g level by using optimized structure of $dadbH_2$ at the b3lyp/6-311++g** level. Further, optimized geometry at the b3lyp/cep-31 g level was used to optimize the structure of $Cu_2(\mu\text{-dadb})(dadbH)_2$ at the b3lyp/lanl$_2$dz level. Geometries of $Zn_2(\mu\text{-dadb})(dadbH)_2$ and $CuZn(\mu\text{-dadb})(dadbH)_2$ were optimized at the b3lyp/lanl$_2$dz level by replacing both/one copper with zinc from the optimized structure of $Cu_2(\mu\text{-dadb})(dadbH)_2$ at the b3lyp/lanl$_2$dz level. The NBO charges were calculated at the b3lyp/lanl2dz level using optimized structures at the highest level (b3lyp/lanl$_2$dz) for all three complexes.

3. Results and discussion

Solid complexes are stable in air but weakly hygroscopic, gaining some weight on exposure to air with extent of weight gain depending on relative humidity. The complexes decompose at 275–300°C. All complexes are insoluble in common organic solvents such as ethanol, methanol, acetone, chloroform, dichloromethane, ether, and benzene as well as highly polar solvents such as DMF and DMSO. The C, H, and N analyses are well within the range of calculated values. Copper and zinc analyses were also in the calculated range for **5** and **6** by atomic absorption spectrophotometry.

3.1. *Powder X-ray diffraction*

PXRD of **2**–**6** and equimolar mixture of **2** and **3** are presented in Supplementary material (figure S1 a-b). The PXRD of the complexes verifies formation of distinct heterobimetallic complexes rather than mixture of the respective monometallic complexes. Comparison of the PXRD lines of **2** and **3** with that of equimolar mixture to **2** and **3** has been restricted to peaks obtained between 2θ values 12–40° due to the

Downloaded by [Renmin University of China] at 10:42 13 October 2013

presence of distinct lines in this region of diffractograms of all the complexes followed by their comparison with other heterobimetallic complexes. Positions of most diffraction lines of **2** are at different 2θ values than **3** (Supplementary material). Peaks at 2θ values 13.27° m and 14.28° m (m = medium intensity) in PXRD of the mixture matches with those of the characteristic peak positions of **3** at 13.20° and **2** at 14.36°, respectively, however, the intensities of each peak is almost halved. There is a broad weak peak in the diffractogram of **2** at 16.23° and a sharp peak at 16.43° in diffractogram of **3** but equimolar mixture exhibits only one symmetrical weak peak at 16.44°. Thus, the above diffraction lines obtained from equimolar mixture of **2** and **3** indicates that the magnitude of intensities of diffraction peaks of the monometallic complexes **2** and **3** are additive in their equimolar mixture and yield averaged diffraction lines. Similarly, a broad weak peak at 17.79° of **2** and a sharp peak at 17.75° of **3** are averaged to yield a symmetrical broad peak at 17.80° in the mixture. Averaging of peak intensities of individual peaks of **2** and **3** of the mixture is prominently marked between 2θ values 18.40–20.60° and 20.60–24.24° (Supplementary material). The magnitude of intensities of the peaks at 19.31° and 20.48° of **2** and at 19.01, 19.87°, and 20.78° of **3** are averaged to yield a relatively broad and symmetrical peak at peak maxima 19.27° in diffractogram of the mixture. Similarly, the magnitude of intensities of the peaks at 21.68° and 22.95° of **2** and 22.27° and 23.59° of **3** are averaged and yield two peaks at 22.42° and 23.40° in the diffractogram of the mixture to **2** and **3**. The positions of the next two peaks at 25.15° and 27.05° in diffractogram of mixture match with those of **3** found at almost same positions, whereas the peak at 28.30° corresponds to the peak of **2** at 28.26° (Supplementary material). Further, intensities of the three peaks at 32.58, 34.39, and 35.62 of **2** and two peaks at 33.05° and 35.07° of **3** are averaged and yield a broad envelope in the diffractogram of mixture from 2θ values 30.66–37.50°.

Non-match of the PXRD lines of **4** with that of the equimolar mixture indicates that it is not a mixture of **2** and **3** (Supplementary material). The PXRD lines at 2θ values 14.36°, 32.94° and 34.28° in diffractogram of **4** are at almost the same positions as in **2**, whereas the peaks at 2θ values 19.44° and 28.34° in diffractogram of **4** are at slightly higher 2θ values as compared to that of the corresponding peaks of **2**. A well-marked broad and symmetrical peak at 36.36° is present in PXRD of **4**, whereas corresponding peak in **2** is present as much weaker and obtained at significantly lower 2θ value (35.50°). Three symmetrical and sharp peaks are present at 2θ values 21.64° mw, 22.44° w and 23.23° m in PXRD of **4** whereas only two peaks (21.70° m and 22.72° bm) are present in the diffractogram of **2** in 2θ 20.21–24°. Thus, the number and nature of peaks from **4** between 2θ values 20.21–24° neither matches with that of **2** nor that of equimolar mixture of **2** and **3** (Supplementary material, figure S2 a-b), indicating that **4** is a new species. Ignoring slight shifting of some peaks of **4** as compared to that of **2** one can consider that **4** is essentially **2** with some impurity of **3** which is responsible for additional peak at 23.23°. Complex **3** exhibits peaks at 13.20° and 26.74° which are more intense than that of the peak at 22.72°, therefore, for impurities of **3** in **4** there must be additional peaks in the diffractogram of **4** at 13.20° s and 26.74°. The absence of peaks of **4** at 13.20° and 26.74° and non-match of the diffractogram of **4** with that of equimolar mixture indicates that **4** is neither **2** nor a mixture of **2** and **3**, i.e. it has a new identity.

Complex **4** exhibits 12 distinct lines whereas **5** and **6** exhibit 17 and 28 distinct lines between 2θ values 12–40°. Complexes **5** and **6** exhibit sharper diffraction lines than **4**. Thus, the number of lines is different in each complex and their positions do not

coincide with those of equimolar mixture of **2** and **3** and monometallic complexes. These features indicate that **4–6** are new species rather than mixture of monometallic complexes. The distinct identity of **7** has been reported earlier (Supplementary material, figure S6 b) [11].

3.2. *Thermal results*

Thermal studies of **2** and **3** and representative heterobimetallic complexes **4** and **7** were reported earlier [11]. Based on thermal studies we reached the conclusion that the thermal degradations of monometallic **2** (up to ~800°C) and **3** (up to 1200°C) under nitrogen exhibit residue corresponding to half mole of respective metal (for **2** obs. 9.00, Calcd 10.15%; for **3** obs. 11.5, Calcd 11.34%). Thermal degradations of **2** and **3** under air yield a residue corresponding to one mole of CuO (obs. 26.5, Calcd 26.12%) and half mole of ZnO (obs. 13.9, Calcd 14.11%) (Supplementary material).

For equimolar mixture of **2** and **3**, the final residue under nitrogen is calculated to be 10.55%, consistent with composition 1/4 mole of copper and 1/4 mole of zinc metal following respective degradation pattern of **2** and **3**. TGA thermogram of heterobimetallic **4** under nitrogen exhibits a residue 5.3% (Supplementary material) corresponding to composition 1/4 mole of copper. Magnitude of observed residue from TGA of **4** does not match with calculated value for a mixture of their monometallic complexes **2** and **3** under nitrogen. This indicates that **4** is new species rather than equimolar mixture of **2** and **3**. Calculated residue for an equimolar mixture of **2** and **3** under air is 20.27%, matching with the sum of 1/2 mole of copper oxide and 1/4 mole of zinc oxide following respective degradation pattern of the monometallic complexes. However, magnitude of the observed residue (12.62%) from **4** (Supplementary material) under air does not match with magnitude of residue calculated for an equimolar mixture. Magnitude of observed residue matches with half mole of CuO (Calcd 13.05%), indicating that **4** follows a different thermal degradation pattern than a mixture of **2** and **3**, i.e. **4** possesses a distinct identity and is not a mixture of **2** and **3**. Thermal degradation pattern of ligand for the metal complexes is governed by the coordinating metal ion. Thus, metal influences the degradation of ligand through delocalization of metal electron on the ligand via metal-to-ligand π-bonds (i.e. thermal study provides indirect evidence of metal ligand orbital overlap). The metal–ligand π-orbital overlap might be responsible for delocalization of metal electrons on the ligand to yield electrical conductance.

However, **7** exhibits a residue of 11% (Calcd 10.3% for the composition $Cu_{0.03125}Zn_{0.4375}$) and 13.6% (Calcd 13.35% for $Cu_{0.0625}Zn_{0.4375}O_{0.5}$) under nitrogen and air, respectively. Calculated residue for a mixture of **2** and **3** in 1 : 15 molar ratio is 11% and 14.3% under nitrogen and air, respectively, following respective degradation pattern. As magnitude of residue obtained from **7** and those calculated for the mixture of **2** and **3** in appropriate mole ratio are within the range of experimental error, it is difficult to conclude its distinct identity on the basis of thermal study.

3.3. *IR spectra*

The presence of ν(OH) in the IR spectra of metal complexes (Supplementary material) indicates water in the complexes. The presence of only one band corresponding to

Downloaded by [Renmin University of China] at 10:42 13 October 2013

Table 1. Magnetic moment data and electronic absorption bands of the complexes.

Compound	Magnetic moment (BM)	λ_{max} (cm^{-1}) as Nujol mull
1	–	16,722, 22,573, 32,051, 36,316, 37,736, 46,083
2	1.63	16,502, 23,148, 31,847
4	2.03	16,892, 27,933, 40,983, 46,511
5	1.96	17,153, 27,777, 28,901
6	1.88	17,391, 26,317, 28,169, 31,746
7	1.92	17,544, 25,316, 26,455, 28,818, 30,488
3	Diamagnetic	19,011, 25,316, 32,051, 36,765

Downloaded by [Renmin University of China] at 10:42 13 October 2013

ν_{as}(N–H) indicates that one hydrogen atom of NH_2 present in free ligand (Supplementary material) [17] is absent from complexes due to deprotonation. Decrease in wavenumber for the NH stretch of the metal complexes compared to that of the free ligand suggests that nitrogen of NH_2 is involved in coordination. Lowering of ν_{as}(C=O) observed in IR spectra of metal complexes indicates coordination of carbonyl [18, 19]. Thus, IR spectra suggest that N and O of ligand are involved in coordination with metal and water is also present in the complexes. Identical IR spectra of complexes kept after 4 months to a fresh sample indicate that samples are stable for longer period.

3.4. *Magnetic and electronic spectra*

Complex **2** exhibits subnormal magnetic moment (μ_{eff}) due to antiferromagnetic interaction between neighboring copper centers bridged by conjugated ligand [9, 10]. Heterobimetallic complexes show normal magnetic moments (table 1) expected from a metal complex containing one unpaired electron [20, 21]. Increase of magnetic moments of the heterobimetallic complexes as compared to **2** indicate that on dilution of paramagnetic Cu(II) centers by diamagnetic zinc(II) ions the antiferromagnetic interaction was diminished.

Solid state electronic spectra of dadb (**1**) exhibit a broad envelope of absorption from ~14,000 to 29,500 cm^{-1} (~715–340 nm) which encompasses one shoulder ~16,900 cm^{-1} (~590 nm), almost flat region at maximum absorption ~22,500 cm^{-1} (~445 nm) and a broad peak at 31,700 cm^{-1} (~315 nm). Two shoulders are observed at 36,316 (~275 nm) and 37,736 cm^{-1} (~265 nm) and a kink at 46,083 cm^{-1} (~217 nm) (Supplementary material). Thus, dadb absorbs in almost the whole visible region and to a large extent into the UV region. The electronic spectrum of **3** also exhibits a broad envelope from 16,000 to 50,000 cm^{-1} (625–200 nm) which encompasses a shoulder at 19,011 cm^{-1} (~525 nm) and a peak at 25,316 cm^{-1} (~395 nm). Another peak is observed at 31,700 cm^{-1} (~315 nm) and shoulder at 36,316 (~275 nm). On comparison of the absorption curve of **3** with dadb shows that the shoulder at 16,722 cm^{-1} of the ligand undergoes blue shift and is observed at 19,011 cm^{-1}. Similarly, the peak at 22,573 cm^{-1} undergoes a blue-shift and is observed at 25,216 cm^{-1}; the other peaks are observed at similar positions as in the ligand. On coordination with metal the first two absorption peaks of dadb shift to higher wavenumbers (lower wavelengths), probably due to ligand-to-metal charge transfer.

Downloaded by [Renmin University of China] at 10:42 13 October 2013

Complex **2** provides absorption spectrum contributed by ligand absorption and d–d transitions with ligand absorptions stronger than d–d transitions. Complex **2** also exhibits a broad envelope of absorptions from 10,000 to 50,000 cm^{-1} (1000–200 nm) but with a more clearly defined shoulder/peak than that of ligand **1**. Electronic spectrum of **2** exhibits a shoulder at ~16,500 cm^{-1} (~605 nm) and a well-resolved peak at 23,300 cm^{-1} (~430 nm) and the third peak of relatively lower intensity at 31,700 cm^{-1} (~315 nm). The first two peaks of **2** are red-shifted compared to those of **3**. This indicates significant metal-to-ligand charge transfer which compensates the ligand-to-metal charge transfer in **2**. However, the absence of any clearly defined shoulder in the spectrum of **2** for d–d transition indicates that ligand and d–d transitions coincide for **2**. Peak positions due to d–d transitions in square-planar geometry may be proposed for **2** [21, 22]; however, it is not conclusive. For **4**–**7**, the first peak is observed at similar positions as a shoulder and the second peak undergoes blue-shift compared to both **2** and **3** around 28,000 cm^{-1}. It is very hard to predict the geometry of these complexes from their electronic spectra due to interference by ligand absorptions.

3.5. *Computational results*

Geometry optimization for $Cu_2(\mu\text{-dadb})(dadbH)_2 \cdot 4H_2O$ at the b3lyp/cep–31 g level yields a distorted octahedral geometry for both Cu(II) ions; however, anhydrous $Cu_2(\mu\text{-dadb})(dadbH)_2$ (**2′**) at the b3lyp/lanl2dz level produces square-planar geometry (Supplementary material) around both metal ions. Computed M–O (L_2/L_3) bond lengths are slightly longer (0.04 Å) than M–O (L_1) bonds in both complexes. The magnitude of M–O (L) bond lengths are almost in the range of single M–O bond lengths (2.0 ± 0.04 Å) but M–O (OH_2) bond lengths in $Cu_2(\mu\text{–dadb})(dadbH)_2 \cdot 4H_2O$ are much longer (2.40 Å), indicating strong Jahn–Teller distortion in **2**, and coordination of water to copper is weak. Strong axial elongation concluded from ESR spectral results (*vide infra*) corroborates the bond length computational result. The absence of an endothermic peak in the DSC curve of **2** dried *in vacuo* over anhydrous $CaCl_2$ for 20 days confirms the predictions from geometrical optimization that bonding between metal ion and water are weak and water is lost on prolonged drying. Optimized molecular geometries for $Zn_2(\mu\text{-dadb})(dadbH)_2$ (**3′**) and $CuZn(\mu\text{-dadb})(dadbH)_2$ (**4′**) at the b3lyp/lanl2dz level show tetrahedral geometry around zinc(II) ions and square-planar geometry around copper(II) ion (Supplementary material).

The magnitudes of computed NBO charges on N_{25} and N_{26} of bridging L_1 are −0.92 for **3′** (Supplementary material). Similarly NBO charges on terminal L_2 (N_{27}) and L_3 (N_{29}) are equal (−0.98). Magnitude of NBO charges on N_{27} and N_{29} are higher than those on N_{25} and N_{26}, whereas all coordinated N and O donors of **3′** and **2′** are expected to exhibit equal magnitude NBO charges. This may be explained by enolization of carbonyl in amino group. When the lone pair electrons of N_{28}/N_{30} is strongly involved in conjugation, the carbonyl bearing O_{21}/O_{23} of **3′** will undergo strong enolization and non-bonded N_{28}/N_{30} will possess the least negative charge. Smallest magnitude of computed NBO charge (−0.74) on N_{28}/N_{30} of **3′** supports enolization of carbonyl in conjugation with amino. With small involvement of lone pair of N_{27}/N_{29} into conjugation with O_{22}/O_{24}, most negative charge will remain localized on N_{27}/N_{29}. Highest computed negative charge (−0.98) on N_{27}/N_{29} of **3′** favors negligible involvement of lone pair electrons of N_{27}/N_{29} for enolization of non-bonded carbonyl

Downloaded by [Renmin University of China] at 10:42 13 October 2013

bearing O_{22}/O_{24}. Smaller bond length (1.268 Å) of C_{16}–O_{24}/C_{10}–O_{22} compared to that of C_{13}–O_{23}/C_7–O_{21} (1.288 Å) also support less enolization of carbonyl bearing O_{22}/O_{24} as compared to that of the carbonyl bearing O_{21}/O_{23} of **3′**. Similarly, moderate enolization of carbonyl of bridging L_1 favors intermediate magnitude of NBO charges computed for N_{25} and N_{26}. Sigma bond (ligand → metal) as well as π-back bond (metal → ligand) are possible between Zn(II) and N_{25}/N_{26} of bridging L_1 as they are coplanar; however, only σ (ligand → metal) bond is feasible between Zn(II) and N_{27}/N_{29} of terminal L_2/L_3 because they are non-planar. On significant metal → ligand π-back bonding, the magnitude of negative charge on N_{25}/N_{26} should increase. Consequently the negative charge on N_{25}/N_{26} should be equal to, or greater than, that on N_{27}/N_{29} but this is not observed. Therefore, considering the trend of NBO charges on various donors it may be concluded that metal → ligand π-back bonds in **3′** are less significant than σ-bonds. Larger bond lengths (1.30 Å) of C_3–O_{19}/C_6–O_{20} than those of C_{16}–O_{24}/C_{10}–O_{22} and C_{13}–O_{23}/C_7–O_{21} indicate higher enolization of C_3–O_{19}/C_6–O_{20} in contrast to the conclusion drawn from NBO charge distribution on nitrogen atoms.

Magnitude of NBO charges on non-coordinating N_{28} and N_{30} of **2′** is almost the same as on **3′**. Trend of magnitude of NBO charges on coordinated nitrogen of **2′** is the same as for **3′**. However, magnitude of NBO charge on coordinated atoms of **2′** is smaller than found for **3′**. Lowering of NBO charges on coordinated nitrogen atoms of **2′** is attributed to increased σ donation to Cu(II) as compared to Zn(II), also supported by smaller Cu–N distance in **2′** (Cu_{31}–N_{29}, 1.93 Å; Cu_{31}–N_{25}, 1.95 Å) as compared to that of Zn–N in **3′** (Zn_{31}–N_{29}, 2.006 Å; Zn_{31}–N_{25}, 2.04 Å). Non-coordinated N_{28} and N_{30} of **4′** possess almost the same NBO charges as on **2′** and **3′**; however, N_{25} and N_{29} of **4′** coordinated to Zn(II) exhibit slightly lower charges than those of corresponding atoms of **3′** and N_{26} and N_{27} of **4′** coordinated to Cu(II) show slightly increased charges as compared to those of **2′**. Thus, bridging N_{25} and N_{26} in **4′** possess different NBO charges; N_{25} bonded with Zn(II) possesses higher charge (−0.908) than N_{26} coordinated to Cu(II) (−0.837).

Distribution of NBO charges on various oxygen atoms also can be explained on the basis of extent of enolization of carbonyl in conjugation with amino of the ligand. Charges on O donors of **2′** as well as **3′** exhibit similar trends as N donors except coordinated O_{19}/O_{20} of bridging L_1 possesses higher charge than that of coordinated O_{21}/O_{23} of terminal L_2/L_3 in contrast to the trend of NBO charges on N donors of **3′**. Carbonyl is capable to accept electron density donated by metal (metal → ligand bonding), provided symmetry of metal and ligand orbitals is matching. Zn(II) and bridging L_1 bearing O_{19}/O_{20} are coplanar in optimized geometry; therefore, NBO charges on these atoms increase. However, Zn(II) and O_{21}/O_{23} are not coplanar so π-back bonding does not take place between Zn(II) and O_{21}/O_{23}. Consequently atomic charge on O_{21}/O_{23} is lower than that on O_{19}/O_{20}. π-Back bonding decreases negative charge on metal ion, enhancing σ-bonding (ligand → metal charge transfer). Due to mutual enhancement of σ and π-back bonding, the enolization of C_3–O_{19}/C_6–O_{20} may increase. Larger bond length (1.30 Å) computed for C_3–O_{19}/C_6–O_{20} than those of C_{16}–O_{24}/C_{10}–O_{22} (1.268 Å) and C_{13}–O_{23}/C_7–O_{21} (1.288 Å) of **3′** corroborate the finding from NBO charges. Thus distribution of NBO charges on donors indicate significant metal → ligand charge transfer on those carbonyl oxygen atoms which are coplanar with Zn(II) in **3′**. π-Back bonding is expected to be the same on all coordinated oxygen atoms in **2′** as Cu(II) and all O donors are coplanar. Magnitude of negative charges on O_{19}/O_{20} are more than on O_{21}/O_{23}, whereas reverse trend is expected on the basis of

Downloaded by [Renmin University of China] at 10:42 13 October 2013

extent of enolization of carbonyl group of **2′**. More enolized carbonyl will have more single-bond character and appear to possess less tendency to accept π electrons *via* π-back bonding. Carbonyl bearing O_{21}/O_{23} has been concluded to exhibit highest enolization therefore and smaller metal → ligand charge transfer than that of carbonyl with O_{19}/O_{20}; consequently, O_{21}/O_{23} possesses lower NBO charges than O_{19}/O_{20} of **2′**. Computed negative charges on donors result from extent of enolization and π-back bonding capacity. Oxygen donor coordinated to Zn(II) in **4′** possess similar magnitude of NBO charges as on pertinent atoms of **3′** and those coordinated to Cu(II) exhibit similar magnitude of negative charge as on pertinent atoms of **2′**.

Replacing Zn_{32} of **3′** by Cu(II) results in formation of **4′**. Thirty out of 46 atoms of **4′** acquire unpaired electron with α-spin (Supplementary material); the remaining 16 atoms have β-spin (C_9, C_{17}, C_{18}, O_{19}, O_{22}, N_{25}, N_{29}, N_{30}, Cu_{32}, Cl_{34}, Cl_{37}, Cl_{38}, H_{39}, H_{41}, H_{43}, and H_{44}). Magnitude of unpaired electron populations on C, H, and Cl are small as compared to those on Cu(II), O, and N. Substitution of Zn_{31} of **4′** by Cu(II) results in **2′**. NBO charges for **2′** show that 36 out of 46 atoms exhibit unpaired electron with α-spin and the remaining 10 have β-spin (N_{28}, N_{30}, Cu_{31}, Cu_{32}, Cl_{35}, Cl_{38}, H_{43}, H_{44}, H_{45}, and H_{46}). N_{30}, Cu_{32}, Cl_{38}, H_{43}, and H_{44} possess unpaired electron with β-spin in **2′** as well as **4′**; however, the magnitude of unpaired electron population on atoms of **2′** is higher than those of corresponding atoms of **4′**. Eleven atoms out of 16 exhibiting unpaired electron with β-spin in **4′** (C_9, C_{17}, C_{18}, O_{19}, O_{22}, N_{25}, N_{29}, Cl_{34}, Cl_{37}, H_{39}, and H_{41}) switch to α-spin in **2′**. N_{28}, Zn_{31}/Cu_{31}, Cl_{35}, H_{45}, and H_{46} showing α-spin in **4′** switch to β-spin in **2′**. All N and O donors of **2′** possess α-spin, whereas O_{19}, O_{22}, N_{25}, N_{25}, and N_{30} of **4′** possess β-spin. Thus, more atoms of heterobimetallic **4′** exhibit β-spin than **2′**.

Total magnitudes of unpaired electrons with α-spin ($U+\alpha$) and β-spin ($U+\beta$) on positively charged atoms of **4′** are smaller than those of **2′**, whereas on negatively charged atoms amount with α-spin ($U-\alpha$) and β-spin ($U-\beta$) is reversed. Net unpaired electrons on various atoms of **4′** per Cu(II) (1.1005) is larger than that of **2′** (1.0672) irrespective of sign and charge (Supplementary material). O_{19} and O_{20} of **2′** possess equal magnitude of unpaired electrons ($U-\alpha$, −0.117) with α-spin, whereas O_{19} and O_{20} of **4′** possess unpaired electron with ($U-\beta$, 0.00137) β-spin and ($U-\alpha$, −0.1182) α-spin, respectively. Increase of unpaired electrons on O_{19} of **2′** as compared to **4′** along with inversion of electron spin ($U-\beta$, 0.00137 → $U-\alpha$, −0.1182) indicates two sources of unpaired electrons on O_{19} of **2′**; one from Cu_{32} and the other from Cu_{31} and the magnitude of computed spin is the summation of both. Due to similar reason O_{20} of **2′** exhibits lower magnitude unpaired electron than that of **4′**. The same trend is observed for the computed magnitude of unpaired electrons on N_{25} and N_{26} of **2′** and **4′**. Thus, larger magnitude of net unpaired electron present on various atoms of **4′** than **2′** is found because a part of unpaired electron generated by Cu_{32} is counterbalanced by that of Cu_{31} in **2′**. This slight excess of unpaired electron on **4′** may be responsible for its different behavior than **2′** and **3**.

3.6. *ESR spectral results*

Owing to the insolubilities of the metal complexes only solid state ESR spectra have been recorded. Room temperature solid state ESR spectrum of **2** exhibits an axial spectrum with a very broad peak corresponding to a parallel and a relatively narrow

Table 2. ESR spectral data of **2**, **4**, and **7**.

Complex	Temperature	$A_{\parallel}$ (G)	g_{av}	$g_{\parallel}$	$FWH_{\parallel}$ (G)	$g_{\perp}$	$FWH_{\perp}$ (G)	Frequency (GHz)	$H_{ref.}$ (TCNE) (G)
2	Room temperature	–	2.097	2.203	230	2.044	100	9.1	3240
2	LNT	–	2.0975	2.203	230	2.0437	90	9.1	3245
4	Room temperature	–	2.098	2.188	290	2.054	148	9.1	3348
7	Room temperature	145	2.127	2.284	320	2.048	90	9.5	3370

Nitrogen super hyperfine = 30 G.

Downloaded by [Renmin University of China] at 10:42 13 October 2013

peak for the perpendicular features (Supplementary material, figure S5). Non-resolution of copper hyperfine coupling constant arises from line broadening as a consequence of smaller spin lattice relaxation time and/or significant spin–spin exchange interaction in the solid state. Liquid nitrogen temperature (LNT) ESR spectrum of **2** is almost identical to that of room temperature ESR spectrum (table 2). The trend $g_{\parallel} > g_{\perp} > g_e$ (free electron value) indicates that free electron resides in the $d_{x^2-y^2}$ orbital of copper in the complex. Pattern of g values and appreciable differences between $g_{\parallel}$ and $g_{\perp}$ values indicate strong Jahn–Teller distortion around copper and the effective geometry around copper(II) is almost square-planar [23–25].

The room temperature solid state ESR spectrum of **4** is very similar to that of **2**. Full-width half-height (FWH) value for **4** is greater than that of **2** for parallel and perpendicular features. Increase in FWH values may be due to partial reduction of line broadening. Reduction of line broadening for **4** arises from reduction of spin–spin exchange interactions on dilution of the magnetic center {copper(II)} by non-magnetic {zinc(II)} in **4** as compared to **2**. A mixture of monometallic complexes is expected to exhibit ESR signal identical to that of **2**, therefore, it may be concluded that **4** has different identity and is not a mixture of **2** and **3**. Room temperature solid state ESR spectrum of **7** is entirely different from those of **2** and **4**, exhibiting an axial spectrum with a well-resolved parallel hyperfine splitting (Supplementary material). Due to strong dilution of magnetic Cu(II) centers by non-magnetic zinc(II) ions in **7** spin–spin exchange interaction between magnetic nuclei is reduced, and line broadening of ESR signal is minimized resulting in resolution of observed hyperfine lines of Cu(II). This observation confirms that copper(II) in **7** is surrounded by non-magnetic zinc(II) ions, consequently, it may be concluded that heterobimetallic **7** is not a mixture of **2** and **3** in appropriate mole ratio. Concentration of Cu(II) is in the order **2** > **4** > **7**, therefore, spin–spin interaction is **7** < **4** < **2**. Due to reduction of spin–spin interaction **4** shows increase in FWH of its EPR signals, whereas **7** exhibits well-resolved copper hyperfine lines in its ESR signal. Nitrogen super hyperfine splitting is also partially visible in parallel features, indicating delocalization of unpaired electron of copper onto nitrogen of the ligand. The presence of unpaired electron on N of the ligand obtained from the NBO analysis corroborates the experimental finding from ESR. Nitrogen super hyperfine lines appear as a consequence of transfer of unpaired electron from Cu(II) → N, therefore, metal → ligand charge transfer concluded from the NBO analysis is corroborated experimentally from ESR. Further, the conclusion drawn from IR spectra that nitrogen of NH_2 is involved in bond formation with metal is supported by the presence of nitrogen super hyperfine lines in ESR spectra of **7**.

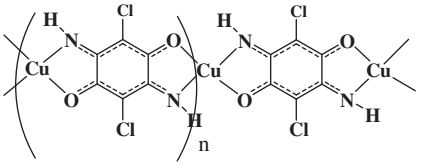

Complex **2**

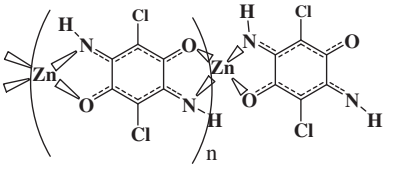

Complex **3**

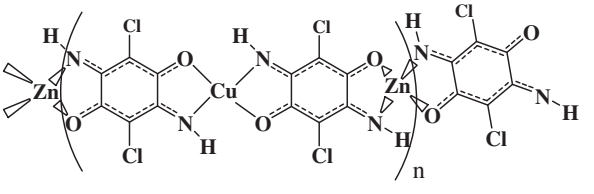

Complex **4**

Figure 1. Proposed structures for **2–4**.

Based on electronic, geometry optimization, and ESR spectral studies, a tetrahedral polymeric 1-D structure for **3**, square-planar 1-D structure [9, 10] for **2**, and 1-D structure possessing square-planar structure around copper and tetrahedral around zinc for **4**–**7** are tentatively proposed (figure 1).

3.7. *Conductivity of the complexes*

Specific conductance of complexes from 313 K to 393 K was measured by the two-probe method using silver paint on compressed pellets prepared at 6 ton pressure and cured at 120°C. Increase in conductivity of all the complexes with increasing temperature indicates that the complexes are semiconductors [2, 26]. Complex **2** exhibits higher conductivity (~10 times) than that of **3** possessing lowest conductivity among all the complexes under present study. Computation of NBO charges on **2′** shows that unpaired electron is delocalized on the conjugated polymer back bone producing lower HOMO–LUMO gap (2.23 eV) than that of **3** (2.47 eV). Higher conductivity of **2** as compared to that of **3** arises from the combined effect of excitation energy (E_g HOMO–LUMO gap) [27], the presence of unpaired electron and coplanar geometry of ligand and metal of **2**. Complex **4** exhibits intermediate conductivity at room temperature between those of **2** and **3** but at higher temperature exhibits higher conductivities than monometallic complexes. Observed conductivity of **4** at room temperature is in the expected range as computed from the HOMO–LUMO gap (2.29 eV) between those of **2** and **3**. Conductivities of **5**–**7** are greater than the conductivities of monometallic complexes with **6** exhibiting highest conductivity at all temperatures (figure 2).

Downloaded by [Renmin University of China] at 10:42 13 October 2013

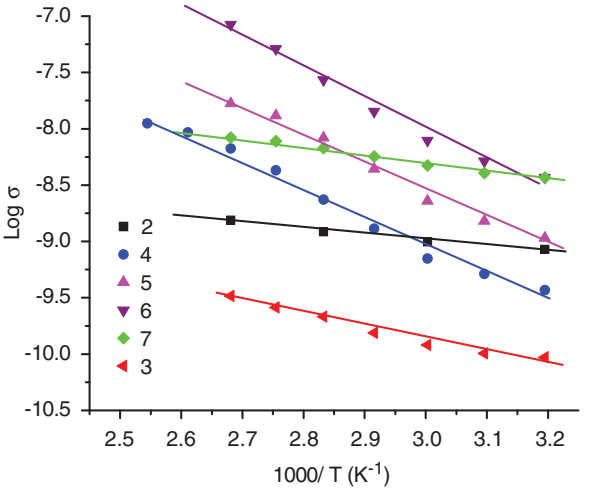

Figure 2. Temperature *vs.* electrical conductivity of **2–7**.

Spin–spin interaction between adjacent metal ions of **2** localizes unpaired electrons of Cu(II) and results in antiferromagnetic interactions; consequently, conductivity of **2** is considerably reduced despite having unpaired electron. ESR spectra also reveal that dilution of Cu(II) with Zn(II) reduces the spin–spin exchange interaction progressively from **4** to **5** to **6** and **7**. Increase in conductivity matches with decreasing spin–spin interaction in the heterobimetallic complexes at room temperature. Due to the presence of insufficient number of carriers in **7** to donate unpaired electron to the conjugated polymeric system, **7** exhibits slightly lower conductivity than **6** with increasing temperature. Observed conductivity of the heterobimetallic complexes are in the order $\mathbf{4} < \mathbf{5} < \mathbf{6} > \mathbf{7}$. Heterobimetallic complexes exhibit higher conductivity than monometallic complexes due to enhanced unpaired electron populations on the conjugated polymeric chain (i.e., on ligand atoms also) rather than being localized on metal as revealed from computational studies and reduced spin–spin interactions observed from ESR spectra.

4. Conclusion

PXRD, ESR spectral lines, and thermal degradation of the complexes indicate distinct identities of the heterobimetallic complexes. ESR spectra and *ab initio* computational results suggest significant metal → ligand charge transfer and greater delocalization of unpaired electron of copper(II) on ligand atoms of heterobimetallic than monometallic complexes. Higher conductivity of **2** than **3** indicates that a partial filled band has been created to some extent in **2** from delocalization of unpaired electron of Cu(II) on various atoms of the conjugated chain. Higher conductivity of heterobimetallic complexes than those of monometallic complexes shows that localization of unpaired electron due to spin–spin interaction is reduced in heterobimetallic complexes. Although the increase in conductivity of heterobimetallic complexes as compared to

Downloaded by [Renmin University of China] at 10:42 13 October 2013

monometallic complexes is significant, but smaller than expected (~100–1000 times), our objective to create partially filled band without redox treatment is fulfilled by incorporation of metal ion having unpaired electron into the chain of conjugated coordination polymer.

Computed geometries around Cu(II) and Zn(II) in heterobimetallic complexes are square-planar and tetrahedral, respectively. Due to non-planarity around Zn(II), unpaired electron of heterobimetallic complexes remains localized. Consequently, movement of electron from one domain to adjacent domains along the conjugated chain cannot take place by orbital delocalization; however, it may take place by hopping mechanism which requires an activation energy. Semiconductor behavior of heterobimetallic complexes supports the above conclusion. The 1-D conjugated polymer having two different metal ions may yield higher conductivity provided both metal ions exhibit similar geometry to allow delocalization of unpaired electron throughout the polymer chain, in addition to reducing spin–spin interaction between adjacent metal ions. Thus, choosing suitable combination of metal ions one may achieve conductivity without complications of redox treatment.

Downloaded by [Renmin University of China] at 10:42 13 October 2013

Supplementary material

Original IR spectra and data, PXRD pattern, Computed NBO charge, unpaired electron population, unpaired electron spin at various atoms of the complexes, optimized structures, UV-visible spectra, TGA thermograms, and original ESR spectra are available in supplementary information file.

Acknowledgments

The authors are grateful to the Head, Department of Chemistry, Banaras Hindu University for providing laboratory facilities. Thanks to SAIF, IIT Chennai and STIC, Cochin, Kerala for recording the DTA and DTA thermograms. SAIF, IIT, Mumbai is gratefully acknowledged for recording ESR spectra. Thanks are also due to Department of Ceramic Engineering IT, BHU for recording PXRD of our samples. Ms Ruchi Pandey from IITR Lucknow is gratefully acknowledged for copper and zinc metal analyses by Atomic Absorption Spectrophotometry. Mr V.N. Panday and S. Tiwari are gratefully acknowledged for recording the IR, electronic spectra, and DSC of our samples. UGC is gratefully acknowledged for providing the financial assistance.

References

[1] C.K. Chiang, C.R. Fincher Jr, Y.W. Park, A.J. Heeger. *Phys. Rev. Lett.*, **39**, 1098 (1977).
[2] J.S. Miller, A.J. Epstein. *Prog. Inorg. Chem.*, **20**, 1 (1976).
[3] W. Knop. *Justus Liebig's Ann. Chem.*, **43**, 111 (1842); W. Knop, G. Schnedermann. *J. Prakt. Chem.*, **37**, 461 (1846).
[4] M.F. Rubner. In *Molecular Electronic*, G.J. Ashwell (Ed.), p. 65, Wiley, New York, NY (1992).

[5] S.S. Zhu, T.M. Swager. *J. Am. Chem. Soc.*, **119**, 12 568 (1997).
[6] C. Creutz, H. Taube. *J. Am. Chem. Soc.*, **95**, 1086 (1973).
[7] M.D. Ward. *Chem. Soc. Rev.*, **24**, 121 (1995).
[8] T. Yamamoto, T. Maruyama, Z-H. Zhou, T. Ito, T. Fukuda, Y. Yoneda, F. Begum, T. Ikeda, S. Sasaki, H. Takezoe, A. Fukuda, K. Kubota. *J. Am. Chem. Soc.*, **116**, 4832 (1994).
[9] S. Kawata, S. Kitagawa, I. Furuchi, C. Kudo, H. Kamesaki, M. Kondo, M. Katada, M. Munakata. *Mol. Cryst. Liq. Cryst.*, **274**, 179 (1995).
[10] B. Wolf, A. Bruhl, V. Pashchenko, K. Removic-Langer, T. Kretz, J.W. Bats, H.-W. Lerner, M. Wagner, A. Salguero, T. Saha-Dasgupta, B. Rahaman, R. Valenti, M. Lang. *C. R. Chim.*, **10**, 109 (2007).
[11] R.L. Prasad, A. Kushwaha, D. Singh. *Thermochim. Acta*, **511**, 17 (2010).
[12] T. Allmendinger. *Macromol. Chem. Phys.*, **198**, 4019 (1997).
[13] B.S. Furmiss, A.J. Hannaford, B. Rogers, P.W.G. Smith, A.R. Tatchell. *Vogel's Text Book of Practical Organic Chemistry*, ELBS 4th Edn, English Language Book Society/Longman (Printed in Great Britain by William Cloves Limited), Beccles and London (1978).
[14] L.F. Fieser, E.L. Martin. *J. Am. Chem. Soc.*, **57**, 1844 (1935).
[15] Y. Matsunaga, C.A. McDowell. *Can. J. Chem.*, **38**, 1167 (1960).
[16] M.J. Frisch, G.W. Trucks, H.B. Schlegel, G.E. Scuseria, M.A. Robb, J.R. Cheeseman, J.A. Montgomery Jr, T. Vreven, K.N. Kudin, J.C. Burant, J.M. Millam, S.S. Iyengar, J. Tomasi, V. Barone, B. Mennucci, M. Cossi, G. Scalmani, N. Rega, G.A. Petersson, H. Nakatsuji, M. Hada, M. Ehara, K. Toyota, R. Fukuda, J. Hasegawa, M. Ishida, T. Nakajima, Y. Honda, O. Kitao, H. Nakai, M. Klene, X. Li, J.E. Knox, H.P. Hratchian, J.B. Cross, V. Bakken, C. Adamo, J. Jaramillo, R. Gomperts, R.E. Stratmann, O. Yazyev, A.J. Austin, R. Cammi, C. Pomelli, J.W. Ochterski, P.Y. Ayala, K. Morokuma, G.A. Voth, P. Salvador, J.J. Dannenberg, V.G. Zakrzewski, S. Dapprich, A.D. Daniels, M.C. Strain, O. Farkas, D.K. Malick, A.D. Rabuck, K. Raghavachari, J.B. Foresman, J.V. Ortiz, Q. Cui, A.G. Baboul, S. Clifford, J. Cioslowski, B.B. Stefanov, G. Liu, A. Liashenko, P. Piskorz, I. Komaromi, R.L. Martin, D.J. Fox, T. Keith, M.A. Al-Laham, C.Y. Peng, A. Nanayakkara, M. Challacombe, P.M.W. Gill, B. Johnson, W. Chen, M.W. Wong, C. Gonzalez, J.A. Pople. *Gaussian 03*, *Revision D.01*, Gaussian, Inc., Wallingford, CT (2004).
[17] R.L. Prasad, A. Kushwaha, Suchita, M. Kumar, R.A. Yadav. *Spectrochim. Acta, Part A*, **69**, 304 (2008).
[18] J.V. Folgado, R. Ibanez, E. Coronado, D. Beltran, J.M. Savariault, J. Galy. *Inorg. Chem.*, **27**, 19 (1988).
[19] K. Nakamoto. *Infrared and Raman Spectra of Inorganic and Coordination Compounds*, 5th Edn, Wiley Interscience, New York, NY (1997).
[20] B.N. Figgis, J. Lewis. *Prog. Inorg. Chem.*, **6**, 37 (1964).
[21] F.A. Cotton, G. Wilkinson, C.A. Murillo, M. Bochmann. *Advanced Inorganic Chemistry*, 6th Edn, Wiley, New York, NY (1999).
[22] A.B.P. Lever. *Inorganic Electronic Spectroscopy*, p. 376, Elsevier, Amsterdam (1986).
[23] B.A. Goodman, J.B. Raynor. *Adv. Inorg. Chem. Radiochem.*, **13**, 135 (1970).
[24] R.L. Prasad, A. Kushwaha, B.P.S. Gautam. *J. Coord. Chem.*, **62**, 2983 (2009).
[25] I. Bertini, D. Gatteschi, A. Scozzafava. *Coord. Chem. Rev.*, **29**, 67 (1979).
[26] N. Singh, S. Gupta. *Synth. Met.*, **107**, 167 (1999).
[27] R.L. Prasad, A. Kushwaha, R. Prasad, S. Jaiswal, R.A. Yadav. *J. Theor. Comput. Chem.*, **8**, 1185 (2009).

Downloaded by [Renmin University of China] at 10:42 13 October 2013